NOTES AND CORRESPONDENCE

Dynamic Boundary Conditions Revisited

GEORGE F. CARNEVALE

Scripps Institution of Oceanography, University of California, San Diego, La Jolla, California

FABIO CAVALLINI

Istituto Nazionale di Oceanografia e di Geofisica Sperimentale–OGS, Trieste, Italy

FULVIO CRISCIANI

Istituto Talassografico del CNR, Trieste, Italy

5 August 1999 and 16 October 2000

ABSTRACT

The applicability of the super-slip boundary condition in wind-driven quasigeostrophic ocean circulation models is reexamined. The energy and enstrophy characteristics of the super-slip condition are discussed for the equilibrium state. A model is constructed with super-slip on the western boundary and free slip on the other boundaries. Both linear and nonlinear solutions are presented. Compared to the case with all free-slip boundaries, this new model gives a more energetic and narrower western boundary current, but otherwise the differences are not very great.

1. Introduction

One of the most important models in the development of the theory of the general circulation of the ocean has been the single-layer quasigeostrophic model with the effect of turbulence parameterized by lateral diffusion of relative vorticity. This turbulence parameterization goes back to Rossby (1936) and its first application to ocean circulation is due to Munk (1950). The equation of evolution for this model is

$$\frac{\partial}{\partial t}\zeta + J(\psi, \zeta) + \beta\frac{\partial \psi}{\partial x} = \frac{1}{H}\,\mathrm{curl}_z\boldsymbol{\tau} - r\zeta + A_H\nabla^2\zeta, \quad (1)$$

where ψ and $\zeta = \nabla^2\psi$ are the streamfunction and the relative vorticity of the large-scale motions of the flow, $\boldsymbol{\tau}$ is the wind stress divided by the density of water, and H is the depth of the fluid. The details of (1) are extensively explained in many textbooks (cf. Pedlosky 1996); here we note only that the forcing is the z component of the wind stress curl, and the $-r\zeta$ represents the effects of Ekman dynamics. The most important point in the present context is that the term with the constant coefficient A_H is the result of turbulence closure modeling. It is derived by averaging over small-scale eddies and replacing the average vorticity eddy flux by the gradient of the large-scale potential vorticity, that is, by setting

$$\langle \mathbf{u}'\zeta' \rangle = -A_H\boldsymbol{\nabla}(\zeta + \beta y), \quad (2)$$

where the primes are used to indicate eddy quantities. On taking the divergence of this term, the lateral diffusion term in (1) is obtained.

For simplicity, the domain for the model will be taken here to be a square box. The natural boundary condition to impose is that of no flow through the boundary, which implies $\psi = 0$ on the boundary. The appearance of the lateral diffusion term requires an additional boundary condition, and there are several possibilities that are often discussed and are referred to as dynamic boundary conditions. Pedlosky (1996) considers four: no-slip $\partial\psi/\partial n = 0$, free-slip (or stress free) $\zeta = 0$, super-slip $\partial\zeta/\partial n = 0$, and hyper-slip $\partial(\zeta + \beta y)/\partial n = 0$, where $\partial/\partial n = \mathbf{n}\cdot\boldsymbol{\nabla}$, and $\mathbf{n}$ is the outward normal on the boundary. Note that, when applied to meridional boundaries, the hyper-slip condition is equivalent to super-slip. Pedlosky emphasizes that there is an important choice to be made here, and the best choice is not obvious a priori. If the lateral viscosity were meant to represent all scales

Corresponding author address: Dr. George F. Carnevale, Scripps Institution of Oceanography, 0213, University of California, San Diego, 9500 Gilman Drive, La Jolla, CA 92093.
E-mail: gfc@castor.ucsd.edu

down to those that actually bring the fluid to rest on the boundary, then the no-slip condition requiring all motion to vanish on the boundaries would be appropriate, but this is not the case when the model only resolves the large-scale motions. For the Laplacian parameterization of small-scale processes used in (1), one cannot declare what the appropriate boundary conditions should be because there is no unique physically correct boundary condition on the large-scale flow. Rather, physical motivation can be used to give preference for one boundary condition or another depending on the circumstances.

Pedlosky (1996) argues that the large-scale flow is buffered by the small-scale processes and should be allowed to slip along the boundary. This would suggest some form of slip boundary condition. The free-slip condition is attractive because it allows no creation of energy on the boundary. But the hyper-slip condition offers a certain consistency with the turbulence modeling that is also attractive. Pedlosky (1996) argues that from the view point of the turbulence closure (2), from which the lateral diffusion was derived, the hyper-slip condition is an appropriate choice. On the boundary, the normal component of the turbulent eddy velocity must vanish, so we have from (2) that

$$0 = \langle \mathbf{n} \cdot \mathbf{u}' \zeta' \rangle = -A_H \mathbf{n} \cdot \nabla(\zeta + \beta y), \tag{3}$$

which gives the hyper-slip condition (Pedlosky 1996).

Furthermore, we can argue that in high Reynolds number flow, a large-scale flow structure moving northward or southward should preserve the potential vorticity ($\zeta + y$) on all of its elements. Consider a region of flow being advected northward along the western or eastern boundary. An element of this flow adjacent to the boundary would have its relative vorticity increasing to compensate for decreasing y. It would seem sensible that the adjacent element of the flow slipping along the boundary should also obey the same conservation law and show an increase in relative vorticity at the same rate. This is accomplished on the western/eastern boundaries by the super-slip condition $\partial\zeta/\partial x = 0$, which forces the adjacent vorticity elements to evolve similarly (cf. Carnevale et al. 1999, 1997).

On the other hand, one of the disconcerting things about the super-slip condition is the possibility of energy creation or loss on the super-slip boundary. The unforced energy evolution equation can be derived from (1) by multiplying by ψ and integrating over the domain to obtain

$$\frac{\partial E}{\partial t} = A_H \oint \zeta \frac{\partial \psi}{\partial n}\, ds - 2A_H Z - 2rE, \tag{4}$$

where $E = \frac{1}{2}\int |\nabla\psi|^2\, dx\, dy$ is the total kinetic energy and $Z = \frac{1}{2}\int \zeta^2\, dx\, dy$ is the total relative enstrophy. Note that the boundary integral on the right-hand side vanishes under the assumption of the free-slip boundary condition on all sides. On a super-slip boundary, the integrand of that integral is of indefinite sign. Nevertheless, as we shall see, a reasonable circulation is possible even if the term acts as an energy source.

Pedlosky (1996) points out that ''we can neglect the eddy flux on the large scale unless we are in regions of the general circulation possessing length scales considerably smaller than the gyre-scale. Such regions do exist near the regions of strong current on the western boundaries of the ocean . . . .;'' Thus it should not make much difference if we choose super-slip or free slip on the eastern boundary, and this is indeed found to be the case. For the work to be presented here, we consider a ''mixed model'' in which we take the super-slip condition on the western boundary and free slip on the remaining boundaries. We will refer to this as the super-slip free-slip (SS–FS) mixed model. We will demonstrate that this mixed model produces reasonable velocity fields, unlike the model with super-slip on all boundaries that Pedlosky (1996) indicates is problematic.

The energetics of the SS–FS model is discussed in section 2. Then, in section 3 we will analyze the linear solution for this model. In section 4, we will compare the fully nonlinear solution of this model to those for the case with free slip on all boundaries.

2. Energetics of the unforced flow

It will prove convenient to rewrite the vorticity evolution equation in nondimensional form as

$$\frac{\partial}{\partial t}\zeta + RJ(\psi, \zeta) + \frac{\partial \psi}{\partial x} = \mathrm{curl}_z \boldsymbol{\tau} - k\zeta + \epsilon\nabla^2\zeta, \tag{5}$$

where the timescale has been taken as $T = (\beta L)^{-1}$, with L the horizontal length scale. The streamfunction is nondimensionalized by UL, and the parameters appearing in the equation are given by $R = U/(\beta L^2)$, $\epsilon = A_H/(\beta L^3)$, and $k = rU/(\beta L)$. Here $\boldsymbol{\tau} = \boldsymbol{\tau}_*/(HUL\beta)$ is nondimensional (asterisk subscripts are used here to indicate dimensional quantities where there may be ambiguity).

As noted in the introduction, the rate of change of the energy for the unforced flow is indeterminate in sign if we adopt super-slip boundary conditions on a portion of the boundary. Nevertheless, as we will see below, for a typical wind forcing the SS–FS model will reach a reasonable equilibrium state. Here we examine somewhat further the energetics of the western boundary in the SS–FS model. The full energy equation with forcing is obtained from (5) by multiplying by ψ and integrating over the domain. The result is

$$\frac{dE}{dt} = -\int \psi\, \mathrm{curl}_z \boldsymbol{\tau}\, dx\, dy - 2kE - 2\epsilon Z + \epsilon \oint \zeta \frac{\partial \psi}{\partial n}\, ds. \tag{6}$$

where the first term on the right-hand side, an integral

over the full domain, is the power generated by the wind forcing. We are concerned with the sign of the last term on the right-hand side, the boundary integral. The integrand vanishes on all boundaries of the SS–FS model except the western boundary. For simplicity, we will take the model geometry to be a square with sides of nondimensional length π. Thus the total boundary integral can be rewritten as

$$\oint \zeta \frac{\partial \psi}{\partial n}\, ds = -\frac{1}{2}\int_0^{\pi} \left(\frac{\partial v^2}{\partial x}\right)_W dy. \tag{7}$$

The subscript W indicates that the quantity in parentheses is evaluated on the western boundary. In the forced equilibrium state, we should expect that the flow will be western intensified, and because the super-slip condition will allow a gradient of v to exist on the boundary, we may anticipate that $\partial v^2/\partial x < 0$ there. This expectation will be verified analytically for the linear solution and numerically for the fully nonlinear solution in the next two sections. Thus the western boundary will typically prove to be a source of energy in the SS–FS model. The equilibrium state energy balance can be written as

$$P - \epsilon\frac{1}{2}\int_0^{\pi} \left(\frac{\partial v^2}{\partial x}\right)_W dy = 2kE + 2\epsilon Z, \tag{8}$$

where P is the power generated by the wind forcing. We have grouped the energy source terms on the left and the sink terms on the right. It is difficult to assess a priori the relative magnitudes of the source and sink terms proportional to ϵ. As we shall see, stationary states can be achieved even when $k = 0$, and so it appears that at least under certain conditions the source term proportional to ϵ will be smaller in magnitude than the sink term.

We next turn to the equation for the enstrophy evolution. From (5), we obtain

$$\frac{dZ}{dt} = P_\zeta - 2kZ - \epsilon\int |\nabla\zeta|^2\, dx\, dy - \frac{1}{2}\oint |\nabla\psi|^2\, dy + \epsilon\oint \zeta\frac{\partial\zeta}{\partial n}\, ds, \tag{9}$$

where P_ζ is the rate of enstrophy input from the forcing. The last integral on the right-hand side of (9) vanishes identically for the SS–FS boundary conditions. The remaining boundary integral involves only dy and, thus, can be rewritten in terms of the meriodional velocity on the eastern and western boundaries. Hence, the enstrophy balance in equilibrium is

$$P_\zeta + \frac{1}{2}\int_0^{\pi} (v_W^2 - v_E^2)\, dy = 2kZ + \epsilon\int |\nabla\zeta|^2\, dx\, dy, \tag{10}$$

where v_W and v_E are the meridional velocities on the western and eastern boundaries, respectively. The integral on the left-hand side would be positive in a western intensified equilibrium flow; hence, again we have sources on the left-hand side and sinks on the right. It is interesting to consider the different origins of the source terms in the energy and enstrophy balances. The western boundary appears as an energy source through a term proportional to ϵ, which is proportional to A_H, a coefficient associated with dissipation. This is not the case for the source term on the right-hand side of (10). If we trace the origin of this source term by referring back to the dimensional equation (1), we see that in dimensional form it would be proportional to β and, hence, is an effect of the variation of the Coriolis parameter with latitude.

3. Linear solution

Here we investigate the linear solution to the wind-forced version of our SS–FS model. For simplicity we will neglect the bottom friction term (i.e., we take $k = 0$). We will adopt the traditional assumption of a latitudinally sinusoidal wind stress curl. We set $\text{curl}_z\boldsymbol{\tau} = -\sin y$ in order to induce a rudimentary subtropical gyre in the domain $D = [0 \le x \le \pi] \times [0 \le y \le \pi]$. Therefore, the stationary form of the vorticity equation (5) reduces to

$$\frac{\partial\psi}{\partial x} = -\sin y + \epsilon\nabla^2\zeta. \tag{11}$$

We look for a solution of the form

$$\psi(x, y) = X(x)\sin y, \tag{12}$$

which automatically satisfies no mass flux ($\psi = 0$) on the meridional boundaries. To satisfy the remaining boundary conditions as well as (11), the problem for $X(x)$ becomes

$$X' = -1 + \epsilon X^{iv} - 2\epsilon X'' + \epsilon X, \tag{13}$$

$$X(0) = X(\pi) = 0, \tag{14}$$

$$X'''(0) = X'(0), \tag{15}$$

$$X''(\pi) = X(\pi), \tag{16}$$

$$X''(\pi) = 0, \tag{17}$$

where we have used (14) in simplifying (16).

To obtain an explicit solution of the problem (13)–(17), we must fix the value of ϵ. Several conditions must be matched. First of all, for this linear problem to be a valid approximation to the full nonlinear problem requires that the Rossby number R be sufficiently small with respect to ϵ. Specifically the linearization is valid when

$$R^{1/2} \ll \epsilon^{1/3}. \tag{18}$$

Thus, if a typical interior current U is $O(10^{-2}\ \text{m s}^{-1})$ with a horizontal length scale $L = O(5 \times 10^5\ \text{m})$ and $\beta = 2 \times 10^{-11}\ \text{m}^{-1}\ \text{s}^{-1}$, then condition (18) becomes

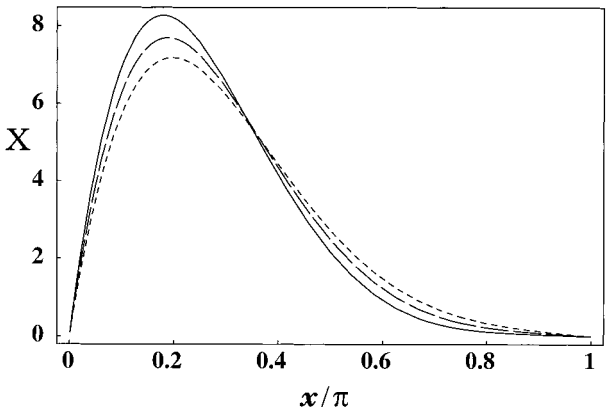

FIG. 1. Graphs of the solutions $X(x)$ for $\epsilon = 0.0695$, 0.0781, and 0.0868 (solid, long dash, and short dash, respectively).

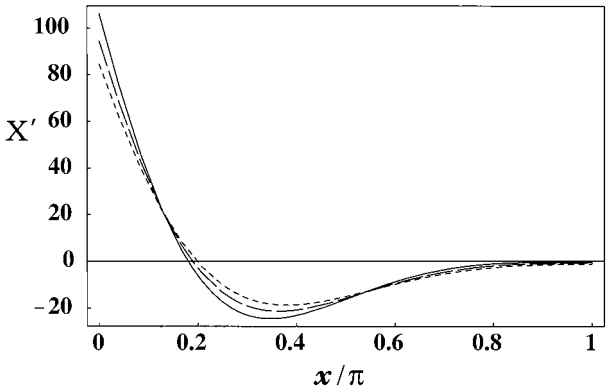

FIG. 2. Graphs of the midlatitude meridional velocity $v = X'(x)$ for $\epsilon = 0.0695$, 0.0781, and 0.0868 (solid, long dash, and short dash, respectively).

$$\epsilon \gg 6.56 \times 10^{-6}. \tag{19}$$

Second, solutions of (13)–(17) with ϵ ''too large'' would tend to smooth the western intensification to the point of producing an almost symmetrical gyre. On the other hand, solutions with ϵ ''too small'' exhibit a secondary gyre in the eastern area of the basin, which is also unrealistic. A trial and error procedure showed that values of ϵ close to 0.0868 give a reasonable solution subject to the constraint of linearity. Graphs of the solutions $X(x)$ are shown in Fig. 1 for $\epsilon = 0.0695$, 0.0781, and 0.0868. We have taken three values of ϵ simply to illustrate the stability of the solution to small variations in ϵ. In Fig. 2, we graph the meridional velocity for the midlatitude line $y = 0$; that is $v = X'(x)$. There we see an intense northward transport near the western boundary that is accompanied by a countercurrent that weakens rapidly with x. For these solutions, we can evaluate two important quantities: the dimensional northward transport M_* that takes place in the western area of the basin and the dimensional meridional current v_* along the western boundary. For simplicity we consider here only the case $\epsilon = 0.0868$. We can estimate M_* by $M_* \approx H\Delta\psi_* = HUL\psi_{\max}$, where H is the depth of the northward moving current and the nondimensional $\psi_{\max}$ is provided by our solution. There is some flexibility in choosing the scales U and L; however, we should keep in mind the constraint that by writing $\text{curl}_z\boldsymbol{\tau} = \sin y$, we have set $\tau_0 = \beta HUL$, where τ_0 is the dimensional magnitude of the wind stress (divided by the density of water), which is typically taken to be $O(10^{-4}\ \text{m}^2\ \text{s}^{-2})$. With $\beta = 10^{-11}\ \text{m}^{-1}\ \text{s}^{-1}$ and $H = O(10^3\ \text{m})$ this implies $HUL = 5$ Sv (Sv $\equiv 10^6\ \text{m}^3\ \text{s}^{-1}$). With $\psi_{\max} \approx 7$, we obtain $M_* \approx 35$ Sv. This value is much larger than those inferred from some classical linear models (Hendershott 1987) but, at the same time, it is very close to that of the Gulf Stream off the Florida coast. Moreover, from $v = X'(x)$ and $X'(0) = 27.029$, we can calculate $v_* = UX'(0)$. Note that fixing the depth $H = 10^3$ m imposes the restriction that $UL = 5 \times 10^3\ \text{m}^2\ \text{s}^{-1}$. Choosing $U = O(10^{-2}\ \text{m s}^{-1})$, which would be a typical eastern basin value, would correspond to taking $L = 5 \times 10^5$ where the domain size is $(\pi L \times \pi L)$. Proceeding with those values leads to $v_* \approx 0.845\ \text{m s}^{-1}$, which is a realistic westward intensified current.

It is interesting to compare $X'(x)$ with the profiles corresponding to the Munk (1950) model using the no-slip condition on the meridional boundaries and free slip along the zonal boundaries, and the Welander (1964) model assuming free-slip boundary conditions on all sides, all with the same value of ϵ. In Fig. 3, we see that the our SS–FS mixed model exhibits very large transport localized in a narrow boundary layer. On the other hand, in order to obtain transport M and current width W of the western boundary current comparable to those of Welander and Munk reported in Table 1 with the SS–FS model, we would need to take values of ϵ considerably higher than 0.0868. This is shown in Table 2 where we give the values obtained from two simulations with the SS–FS model with larger values of ϵ. In one case the results are similar to those for the Munk model, while in the other they are similar to Welander's model results, both using the smaller value of $\epsilon = 0.0868$.

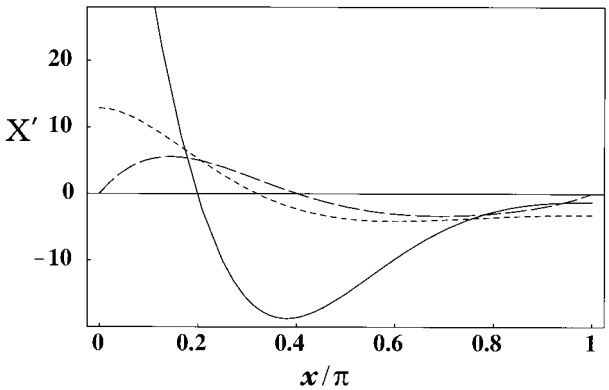

FIG. 3. Comparison of the midlatitude meridional velocity $v = X'(x)$ given by the mixed model (solid), Welander's model (short dash) and Munk's model (long dash) ($\epsilon = 0.0868$ in each case).

TABLE 1. Comparison of the northward transport M and the western boundary layer width W from SS–FS model with the values obtained from the Welander (1964) and Munk (1950) models: W is given in nondimensional units in which the width of the basin is π.

M	W	Model
7.109 Sv	0.198π	SS–FS mixed
2.266 Sv	0.319π	Welander
1.385 Sv	0.402π	Munk

Contour plots of the streamfunction and vorticity from the total solution of (12) are shown in Fig. 4, again for $\epsilon = 0.0868$. We note the north–south reflection symmetry typical of the linear models, and also the westward intensification, which is an immediate consequence of the structure of $X(x)$. For $\epsilon = 0.0868$, the linearized SS–FS model gives a relatively broad flow. In contrast, for smaller values of ϵ the flow is far more confined to the western boundary layer. For example, the streamfunction and vorticity contour plots for the linear solution with $\epsilon = 0.0009$ (shown in Figs. 6a and 7b) are much narrower than those shown in Fig. 4.

Due to the fact that $\zeta \approx 0$ for large x, the gradient of ζ is large only in the area near the western boundary. However, because of the super-slip condition on the western boundary, the isolines of vorticity are orthogonal to the boundary. There must be a meridional strip near the boundary in which $\partial\zeta/\partial x \approx 0$. But this means that $\zeta = F(y)$ in that strip, for some function $F(y)$. Thus, in the strip we have

$$(X'' - X)\,\sin y = F(y), \tag{20}$$

which means that $X'' - X = c$. From condition (14) we have $c = X''(0)$. We can then write a simplified solution in the strip by solving

TABLE 2. These are the values of ϵ that would be needed in the SS–FS model to obtain a northward transport M and a western boundary layer width W close to those of the classical Welander and Munk models in which we use $\epsilon = 0.0868$. The values of M and W are calculated with the SS–FS model. Here, W is given in nondimensional units in which the width of the basin is π.

ϵ	M	W	Notes
0.276	2.277 Sv	0.314π	M and W near Welander's model values
0.443	1.388 Sv	0.366π	M and W near Munk's model values

$$X'' - X = X''(0), \tag{21}$$

$$X(0) = 0. \tag{22}$$

The solutions of (21) and (22) take the form

$$X(x) = (X'(0) + X''(0))\,\sinh(x) - X''(0)[1 - e^{-x}]. \tag{23}$$

Unfortunately, no a priori estimate of $X'(0)$ and $X''(0)$ is possible; however, we can take their values from our full solution and compare the result from (23) to the full solution. These values are $X'(0) = 27.029$ and $X''(0) = -59.1926$. The comparison is shown in Fig. 5, where we see that the full solution and the approximation (23) are essentially the same in the boundary strip $0 \le x \le 0.056\pi$, demonstrating the validity of the approximation in that strip.

Finally, we note that the interior part of the linear solution obtained here is not linear in x. This is rather different than the interior solution obtained from the Sverdrup balance (Pedlosky 1996) that derives from a local balance of the beta term and the wind forcing. In the interior of the Sverdrup solution, X behaves as

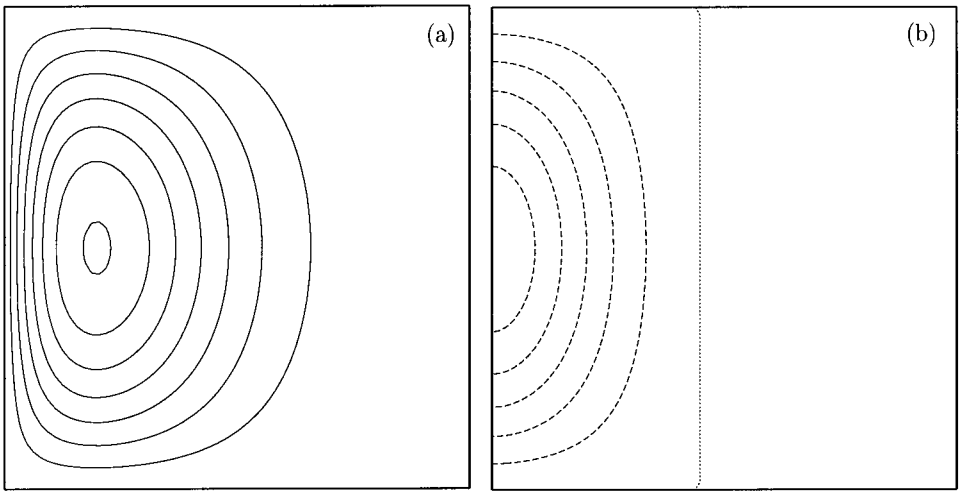

FIG. 4. Contour plots from the linear solution (i.e., $R = 0$) with $\epsilon = 0.0868$ and forcing $\mathrm{curl}_z\boldsymbol{\tau} = -\sin(y)$. The domain size is $\pi \times \pi$. (a) Contour plot of ψ with contour interval 1 in units of UL (see text). The solid lines represent positive valued contour levels. (b) Contour plot of ζ with contour interval 50 in units of U/L. The dashed lines all represent negative valued contour levels. The zero line is dotted. Positive values were insignificant on this scale.

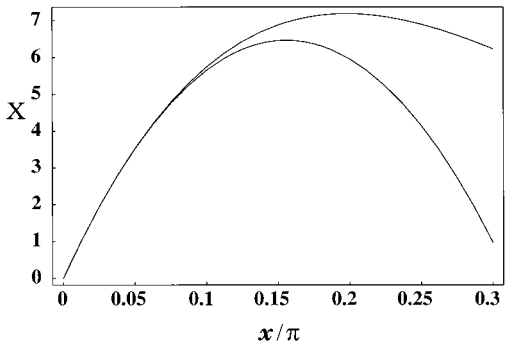

FIG. 5. Comparison between the complete solution $X(x)$ of (13) close to the western boundary (upper graph) and the approximate solution (23) to the approximate problem (21) and (22) in the boundary region. Here we have used the values $X'(0) = 27.029$ and $X''(0) = -59.1926$ taken from the full linear solution ($\epsilon = 0.0868$).

$X(x) = 1 - x$, which is rather different from the behavior seen in Fig. 1. It seems that the super-slip western boundary affects the interior as well as the boundary currents significantly, even in the linear solution. Pedlosky (1996, p. 42) states that there is ''no boundary layer solution possible'' with the super-slip western boundary. Thus, we are unable, with simple analytical methods, to deduce the behavior of M and W as $\epsilon \to 0$. From the numerical simulations here and an additional linear dynamics solution with much smaller ϵ presented in the next section, we can roughly estimate that $W \sim \epsilon^{0.3}$ and $M \sim W^{-1}$.

4. Nonlinear solutions

In this section, we will present some nonlinear solutions obtained with the SS–FS mixed model. We find that qualitatively these solutions are not very different from those obtained with free slip on all boundaries.

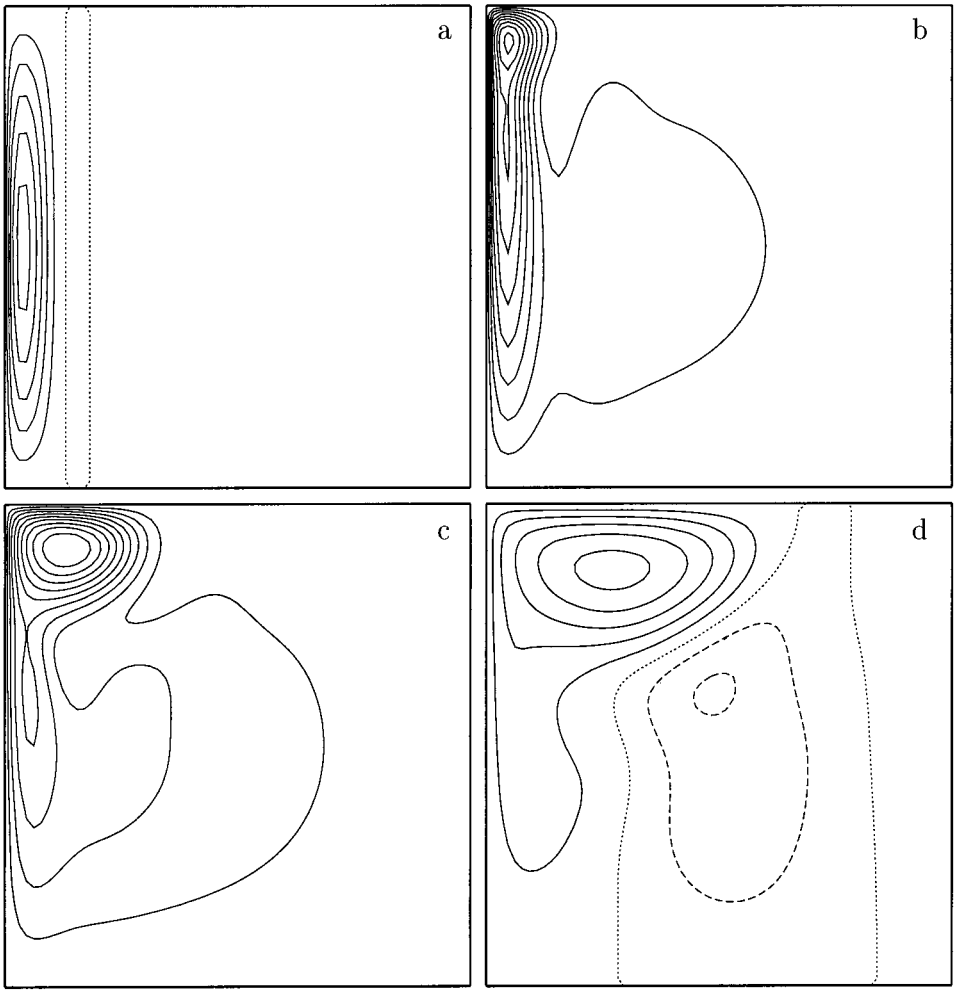

FIG. 6. Contour plots of ψ for $\epsilon = 9 \times 10^{-4}$ and four different values of R. The domain size is $\pi \times \pi$ and the forcing is $\text{curl}_z \boldsymbol{\tau} = -\sin y$ as in Böning (1986). (a) $R = 0$ (contour interval 5), (b) $R = 3.72 \times 10^{-4}$ (contour interval 1.25), (c) $R = 2.33 \times 10^{-3}$ (contour interval 1), and (d) $R = 5.96 \times 10^{-3}$ (contour interval 2). The solid/dotted/dashed lines represent positive/zero/negative valued contour levels.

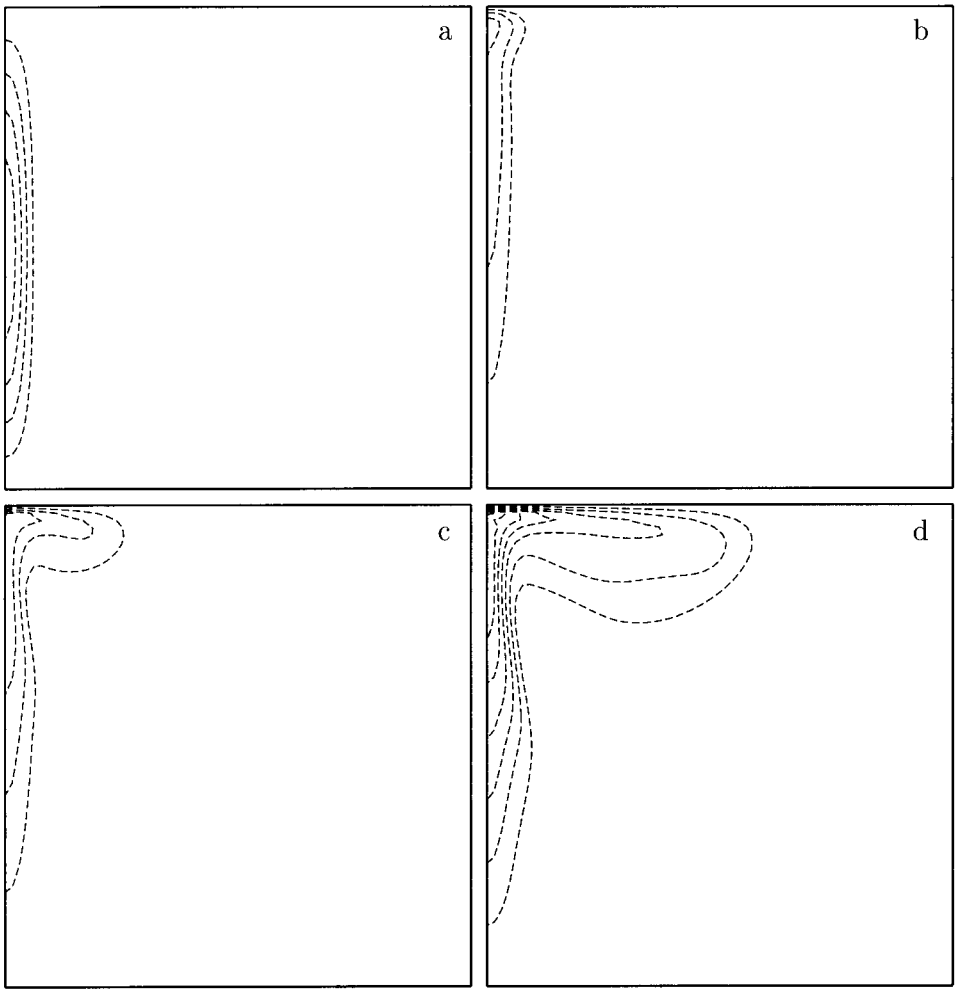

FIG. 7. Contour plots of $\nabla^2\psi$ for $\epsilon = 9 \times 10^{-4}$ and four different values of R. The domain size is $\pi \times \pi$ and the forcing is $\text{curl}_z\boldsymbol{\tau} = \sin y$ as in Böning (1986). (a) $R = 0$ (contour interval 1000), (b) $R = 3.72 \times 10^{-4}$ (contour interval 500), (c) $R = 2.33 \times 10^{-3}$ (contour interval 150), and (d) $R = 5.96 \times 10^{-3}$ (contour interval 50). The dashed lines represent negative valued contour levels. The zero line is not drawn. Positive values were insignificant on this scale.

We will make our comparison with the solutions with free-slip conditions on all boundaries found in Böning (1986), which is a standard reference on the subject (cf. Pedlosky 1996). We obtained our solutions using a finite difference code based on the streamfunction–vorticity formulation. Following Böning, we make the computational domain $D = [\pi \times \pi]$ and apply a wind stress curl given by $\text{curl}_z\boldsymbol{\tau} = \sin y$. In one set of simulations, Böning set the bottom drag coefficient equal to zero and kept the coefficient of lateral diffusion fixed at $\epsilon = 9 \times 10^{-4}$, while varying the value of the Rossby number R. We began by repeating this series of simulations at the same resolution used by Böning (64×64) and found that we could reproduce his results. Then we repeated this series of simulations with the only difference being that the western boundary condition became super slip. The parameters that define Böning's first four experiments are given in Table 3, where the experiment numbers correspond to those used by Böning.[1] Also included in the table are the maximum values for ψ obtained with Böning's model and with our SS–FS mixed model. The streamfunction and vorticity fields for these experiments from our SS–FS model simulations are shown in Figs. 6 and 7.

The streamfunction patterns shown in Figs. 6a–c are steady, while that in Fig. 6d oscillates with the amplitudes of the two cells varying in time. Experiment 1 gives the linear solution (i.e., $R = 0$), and we see in Fig. 6a that the flow is far more confined to the western boundary than in the linear solution presented in the previous section (Fig. 4a), where we used a larger value of ϵ. It is also far more confined to the western boundary than Böning's linear solution (not shown), which is

[1] It appears that the transport value entries for experiments 2 and 3 in Böning's Table I have been mistakenly interchanged.

TABLE 3. The values of R and ψ_{max} in experiments 1–4 of Böning (1986, cf. his Table I). Here we list the nondimensional values for ψ_{max} from Böning's model with free slip on all boundaries and the corresponding values from the mixed model, with a super-slip western boundary. The only parameter varied in this series of experiments was the Rossby number *R*. In each experiment the value of ϵ was fixed at $\epsilon = 9 \times 10^{-4}$ as in Böning's experiments. In experiment 4, the value of ψ_{max} was found to oscillate between 10.6 and 11.7 in the mixed model.

Expt	*R*	ψ_{max} Böning	ψ_{max} SS–FS model
1	0	3.82	27.4
2	3.72×10^{-4}	3.46	11.8
3	2.33×10^{-3}	3.81	9.98
4	5.96×10^{-3}	5.34	10.6–11.7

somewhat intermediate between our mixed model solutions in Figs. 4a and 6a. As the value of *R* increases, our SS–FS model solution becomes less confined, and, in Fig. 6c for $R = 2.33 \times 10^{-3}$ (expt 3), we see a streamfunction that resembles very much that found by Böning for the somewhat higher value of $R = 5.96 \times 10^{-3}$ (expt 4). The oscillating solution with the two gyres in Fig. 6d appears similar in structure to Böning's $R = 9.31 \times 10^{-3}$ case (his expt 5). Considering the vorticity fields displayed in Fig. 7, again we find that the fields are more confined and intense than Böning's results for the same values of *R*. However, if we compare our results to Böning's at somewhat larger values of *R*, then there is a good deal of agreement, at least qualitatively. For example, our vorticity field for experiment 3 is very similar to that of Böning's for experiment 4.[2] So, at least over some broad parameter range, it appears that the SS–FS mixed-model solutions are similar to those with free slip everywhere, but with somewhat larger values of *R*.

It is interesting to note that in establishing a steady state in these cases with no bottom drag, the flow must be such that the input of vorticity is balanced by a viscous diffusion of vorticity through the free-slip boundaries. This can be seen by integrating (5) over the entire domain, which for $k = 0$ gives the result

$$\int \text{curl}_z \boldsymbol{\tau}\, dx\, dy = -\epsilon \oint \frac{\partial \zeta}{\partial n}\, ds. \tag{24}$$

Since $\partial\zeta/\partial n$ vanishes on the western boundary in the SS–FS model, the viscous diffusion necessary for the steady-state balance must occur on the free-slip boundaries. In the nonlinear cases, this diffusion appears to be occurring primarily on the northern boundary (see Figs. 7b,c). This is rather different from what happens in the Munk and Welander models where the diffusion is primarily through the western boundary.

Quantitatively, the SS–FS model gives larger values of the streamfunction and vorticity maxima than Böning's model for the corresponding simulations. For comparison, in Table 3 we have reported the values of ψ_{max} for both Böning's simulations and our SS–FS model. Consider again the case of experiment 3, which has a streamfunction pattern much like that in Böning's experiment 4. In the SS–FS model results for experiment 3, we find $\psi_{max} \approx 10$ in nondimensional units as compared to Böning $\psi_{max} \approx 3.8$ for $R = 2.33 \times 10^{-3}$ (expt 3) or $\psi_{max} \approx 5.3$ for $R = 5.96 \times 10^{-3}$ (expt 4). Using Böning's physical scaling, this would imply a maximum transport in our case, shown in Fig. 6c, of about 100 Sv. This is obtained, following Böning, by assuming the magnitude of the wind stress to be $\tau_0/\rho_0 = 2 \times 10^{-4}$ m^2 s^{-2} and $\beta = 2 \times 10^{-11}$ m^{-1} s^{-1} giving a typical scale for the transport of $HUL = \tau_0/(\rho_0\beta) =$ 10 Sv (cf. Pedlosky 1987, p. 261), and that the total transport would be this times our nondimensional ψ_{max}, as discussed in the previous section. Another reasonable choice for τ_0/ρ_0 would be 1×10^{-4} m^2 s^{-2} (cf. Pedlosky 1986, p. 261), thus reducing our transport to 50 Sv. Alternatively, we note that the values of ψ_{max} are also decreased by the addition of some Ekman damping. In fact, with $k = 9.7 \times 10^{-3}$ and $k = 2.4 \times 10^{-3}$, the two lowest nonzero values used by Böning, we obtain transports of 73 and 50 Sv, respectively, even assuming his higher value of τ_0, while the overall flow pattern remains similar to that in Fig. 6c. Thus, the super-slip boundary condition on the western boundary produces general circulation patterns that are both quantitatively and qualitatively as reasonable as those produced with free-slip on all boundaries. In fact, the super-slip boundary on the western boundary may be said to produce superior results because it produces less damped and more confined boundary currents than the free-slip condition.

5. Conclusions

The strong differences between simulations with all free-slip versus all super-slip boundaries noted in Pedlosky (1996) suggested that the super-slip boundary may not be appropriate for general circulation modeling. This was in spite of the physical argument made by Pedlosky in favor of super-slip as appropriate for the western boundary where the currents are most intense. However, there is no reason why we cannot consider a mixed model with super-slip applied to the western boundary and free slip elsewhere. We have shown that although the linear solution ($R = 0$) with a super-slip western boundary does not give the simple Sverdrup interior solution, it produces, nevertheless, streamfunctions with boundary layer thickness and current intensities that appear physically reasonable both quantitatively and qualitatively. Futhermore, we demonstrated that super-slip western boundary in the mixed model can result in reasonable flows in the wind-forced fully nonlinear experiments suggested by Böning (1985).

One may question whether or not the super-slip con-

[2] The vorticity contour plots for experiments 1 and 2 in Böning's Figs. 3 and 4 have been rotated by ±90°.

dition should be extended to the northern boundary where the currents can also be intense. Recall that Pedlosky's argument was in favor of the hyper-slip boundary condition, which is equivalent to the super-slip condition only on the meridional boundaries. If applied to the northern boundary, the hyper-slip condition would not reduce to super-slip. Without the motivation based on (3), it is difficult to argue for super-slip on the northern boundary, and we have not performed the necessary simulations to comment further on this possibility.

We conclude, on the basis of our numerical and analytical reanalysis of the super-slip condition, that it is premature to rule it out as a western boundary condition for basin-scale modeling.

Acknowledgments. GFC wishes to thank the Istituto Talassografico del CNR for its hospitality during his visit to Trieste. GFC also gratefully acknowledges support for this work from the Office of Naval Research (Grants N00014-96-1-0065 and N00014-97-0095). We thank Glenn Ierley and Vitalii Sheremet for providing the code used to obtain the nonlinear solutions discussed above. We also thank W. R. Young for some guidance on boundary layer theory.

REFERENCES

Böning, C. W., 1986: On the influence of frictional parameterization in wind-driven ocean circulation models. *Dyn. Atmos. Oceans,* **10,** 63–92.

Carnevale, G. F., O. V. Fuentes, and P. Orlandi, 1997: Inviscid dipole-vortex rebound from a wall or coast. *J. Fluid Mech.,* **351,** 75–103.

——, S. G. Llewellyn Smith, F. Crisciani, R. Purini, and R. Serravall, 1999: Bifurcation of a coastal current at an escarpment. *J. Phys. Oceanogr.,* **29,** 969–985.

Courant, R., and D. Hilbert, 1953: *Methods of Mathematical Physics.* Vol. 1. Wiley-Interscience, 560 pp.

Hendershott, M. C., 1987: Single layer models of the general circulation. *General Circulation of the Ocean,* H. D. Abarbanel and W. R. Young, Eds., Springer-Verlag, 291 pp.

Munk, W. H., 1950: On the wind-driven ocean circulation. *J. Meteor.,* **7,** 79–93.

Pedlosky, J., 1987: *Geophysical Fluid Dynamics.* Springer-Verlag, 710 pp.

——, 1996: *Ocean Circulation Theory.* Springer-Verlag, 453 pp.

Rossby, C. G., 1936: Dynamics of steady ocean currents in the light of experimental fluid mechanics. Pap. Phys. Oceanogr. Meteor. No. 5, Massachusetts Institute of Technology and Woods Hole Oceanographic Institution, 43 pp.

Welander, P., 1964: Note on the role of boundary friction in the wind-driven ocean circulation. *Tellus,* **16,** 408–410.